

Of Floquet Topological Insulator

Physics

Of Floquet Topological Insulator

1 Floquet Theory

2 (111) bilayer- ABO_3 structure

2.1 Perovskite structure ABO_3

2.2 Theoretical calculation of the (111) bilayer LaNiO_3

2.3 Model and Method

2.4 Periodic driven under a Laser field

3 The quantitatively description of energy bands with different parameters

4 Semiconductor quantum well structure

4.1 Basic features of HgCdTe quantum well

4.2 model and method

4.3 Experimental realization

5 Preliminary Knowledge

5.1 The inverted energy level in HgTe

5.2 Slater-Koster method

5.3 The rotating-wave approximation

1 Floquet Theory

- the solutions to the time-dependent Schrodinger's equation

$$\hat{H}(t)|\psi(t)\rangle = i\hbar\partial_t|\psi(t)\rangle, \quad \text{with} \quad \hat{H}(t+T) = \hat{H}(t)$$

$$|\psi_{k\alpha}(t)\rangle = e^{-i\epsilon_{k\alpha}t}|\phi_{k\alpha}(t)\rangle$$

where α index the two orbitals per site and two sites in the bilayer unit cell.

2 (111) bilayer- ABO_3 structure

2.1 Perovskite structure ABO_3

- Geometry
- Thermal properties
- Applications

2.2 Theoretical calculation of the (111) bilayer LaNiO_3

- The basic parameters and notations

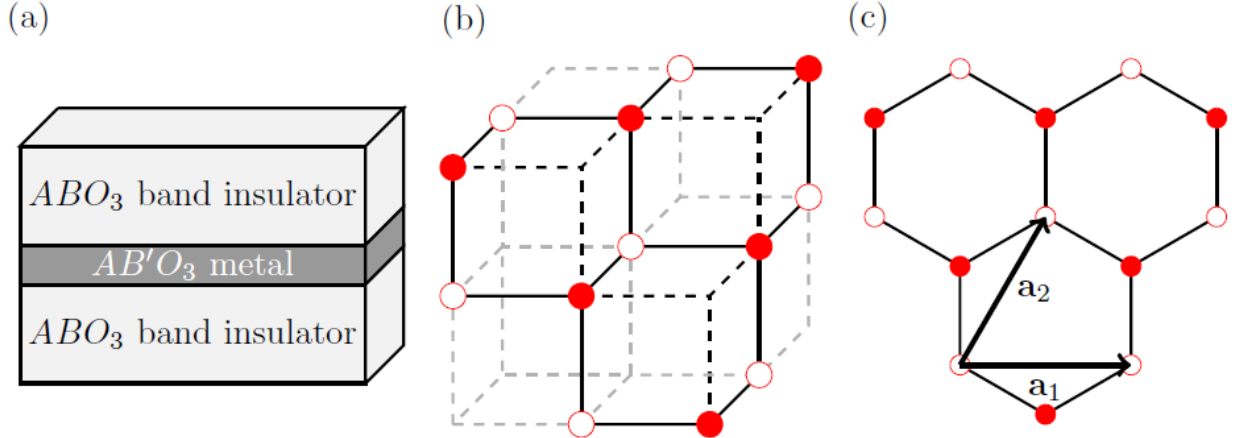


FIG. 1. (Color online) (a) Transition metal oxide heterostructure grown along (111) direction of the form $AB'O_3/ABO_3/AB'O_3$. The shaded area consists of the (111) bilayer LaNiO_3 , and the light area consists of the non-magnetic band insulator LaAlO_3 . (b) The locations of the transition metal ions Ni in (111) bilayers of perovskite structured LaNiO_3 are shown. Filled (open) circles represent ions in top (bottom) layer. The lattice constant is $a_0 = 3.82\text{\AA}$. (c) Buckled honeycomb lattice formed in the (111) bilayer LaNiO_3 . The lattice constant is $\tilde{a} = \sqrt{2/3}a_0 = 3.12\text{\AA}$. The primitive lattice vectors are chosen as $\mathbf{a}_1 = (\sqrt{3}, 0)\tilde{a}$, $\mathbf{a}_2 = (\sqrt{3}/2, 3/2)\tilde{a}$. For convenience, an additional vector is defined as $\mathbf{a}_3 = \mathbf{a}_2 - \mathbf{a}_1$.

- Lattice vectors:

$$\vec{a}_1 = \tilde{a}(\sqrt{3}, 0), \vec{a}_2 = \tilde{a}\left(\frac{\sqrt{3}}{2}, \frac{3}{2}\right), \vec{a}_3 = \vec{a}_2 - \vec{a}_1 = \tilde{a}\left(-\frac{\sqrt{3}}{2}, \frac{3}{2}\right)$$

- Reciprocal lattice vectors

$$\vec{b}_1 = \frac{2\pi}{\tilde{a}}\left(\frac{\sqrt{3}}{3}, -\frac{1}{3}\right), \vec{b}_2 = \frac{2\pi}{\tilde{a}}\left(0, \frac{2}{3}\right)$$

- Three nearest neighbor vectors (from an open point to three solid points):

$$\delta_x = \tilde{a}\left(-\frac{\sqrt{3}}{2}, -\frac{1}{2}\right), \delta_y = \tilde{a}\left(\frac{\sqrt{3}}{2}, -\frac{1}{2}\right), \delta_z = \tilde{a}(0, 1)$$

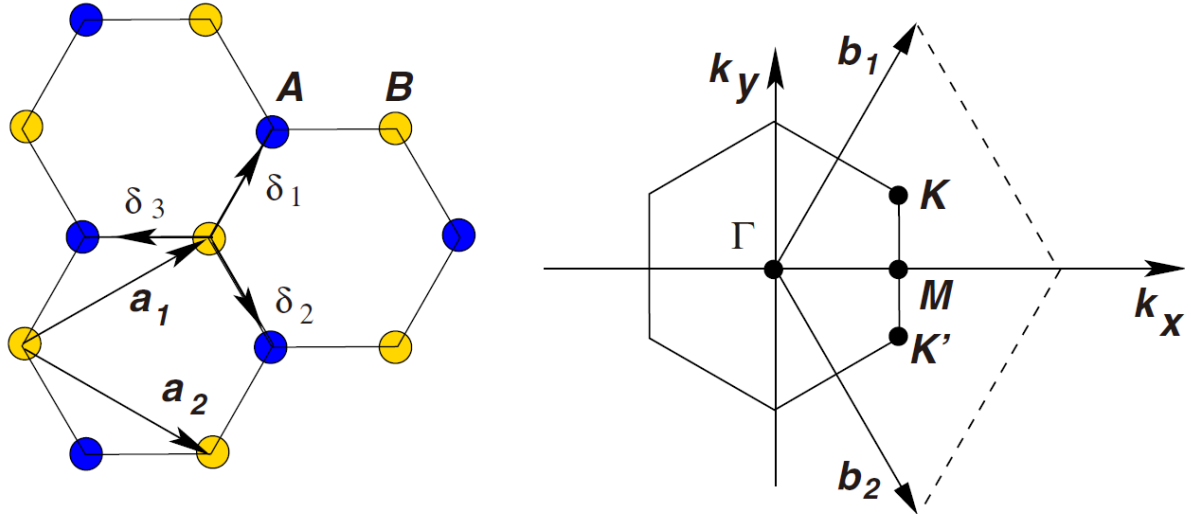
- Special points

$$\text{Dirac points : } \vec{K} = \frac{2\pi}{\tilde{a}}\left(\frac{2\sqrt{3}}{9}, 0\right) = \frac{2}{3}\vec{b}_1 + \frac{1}{3}\vec{b}_2, \quad \vec{K}' = -\vec{K}$$

$$\text{Quadratic points : } M_{\pm} = \frac{2\pi}{\tilde{a}}\left(0, \pm\frac{1}{3}\right) = \pm\frac{1}{2}\vec{b}_2$$

- Incident direction

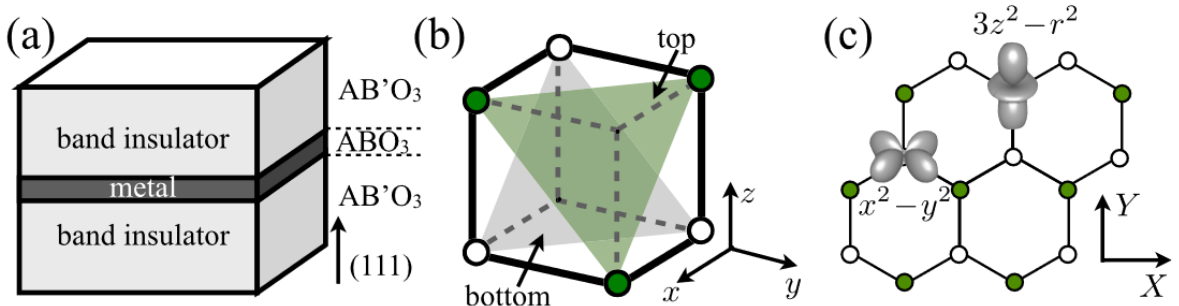
In order to clearly exhibit the effect of the laser on the quadratic touching and Dirac points, the Floquet-Bloch electronic band structures are along the path $\mathbf{K}' - \Gamma - \mathbf{K}$ or $\mathbf{M}_{-} - \Gamma - \mathbf{M}_{+}$.



2.3 Model and Method

- The generalized tight-binding model

[Ref: Gregory A. Fiete and Andreas Rüegg, 2015, *Topological phases in oxide heterostructures with light and heavy transition metal ions*]



$$\begin{aligned} \hat{H} = & \sum_{\vec{R} \in A} \sum_{u=xyz} [d^\dagger(\vec{R}) t_u d(\vec{R} + \delta_u) + h.c.] \\ & + \sum_{\vec{R} \in A} \sum_{u=xyz} [d^\dagger(\vec{R}) t_{u,u+1} d(\vec{R} + \delta_u - \delta_{u+1}) + h.c.] \\ & + \sum_{\vec{R} \in B} \sum_{u=xyz} [d^\dagger(\vec{R}) t_{u,u+1} d(\vec{R} - \delta_u + \delta_{u+1}) + h.c.] \end{aligned}$$

where $d^\dagger = (d_{3z^2-r^2}^\dagger, d_{x^2-y^2}^\dagger)$

- Ni* : $[3d^8 4s^2] \quad ^3F_4$
- e_g*-Orbital model for the (111) bilayer

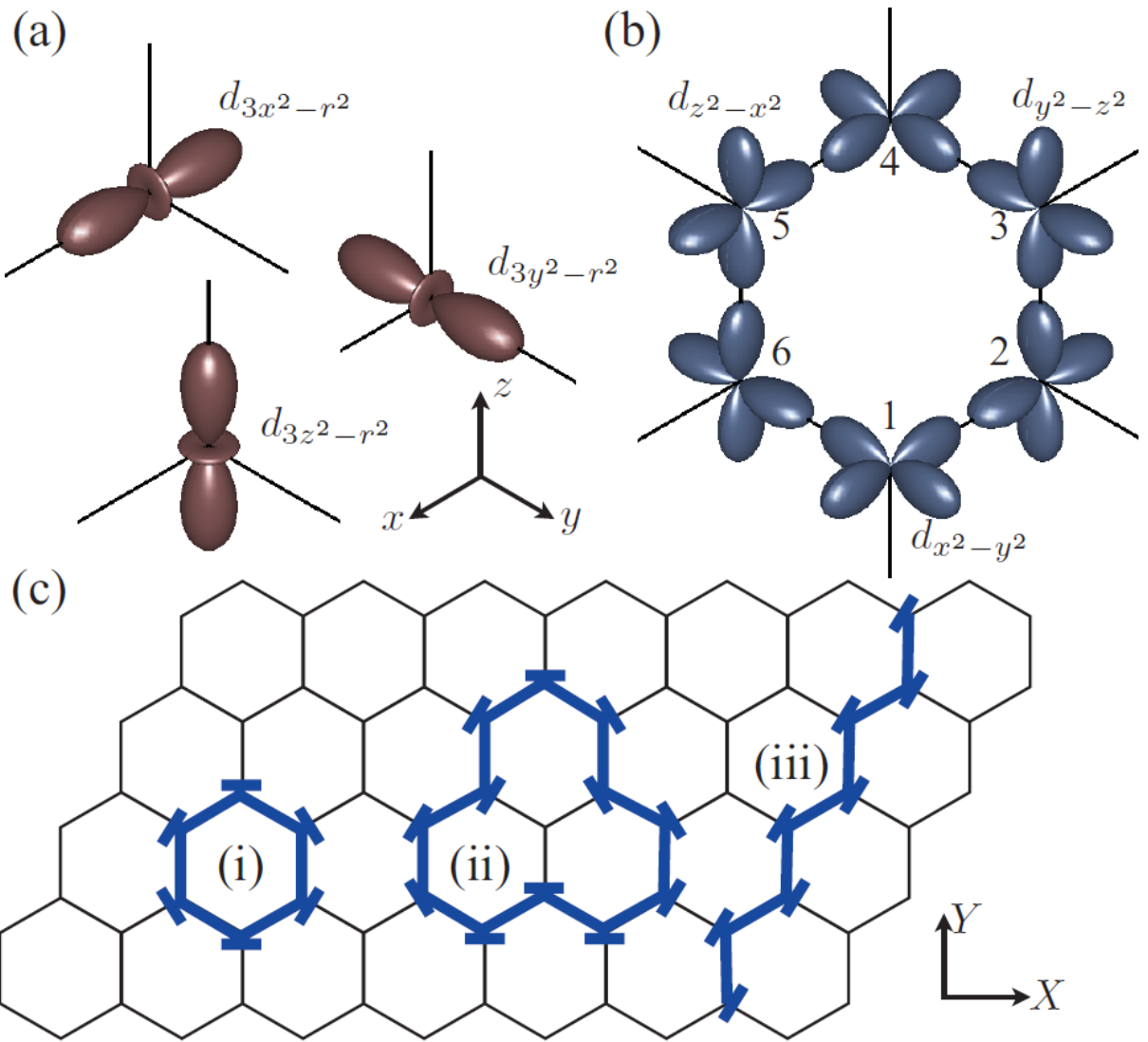
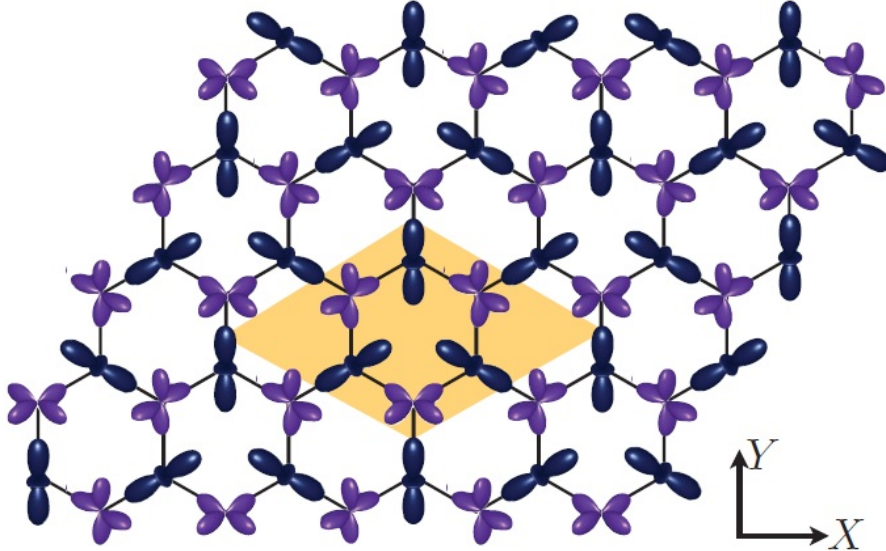


FIG. 5. (Color online) (a) Oxygen mediated hopping along the principal axis of the cube is between the $d_{3u^2-r^2}$ orbitals with $u = x, y, z$. (b) A spatially localized eigenstate of the nearest-neighbor tight-binding model Eq. (2). The viewpoint is along $[111]$. (c) Taking equal-weight superpositions of the hexagonal states (i) allows one to construct localized states with support on arbitrary contractible loops (ii). There are two more states which are linearly independent from the hexagonal states and have support on a loop encircling the torus in one or the other direction (iii).



- The nearest neighbor hopping matrices:

$$t_x = -\frac{1}{4} \begin{pmatrix} t_\sigma + 3t_\delta & \sqrt{3}(t_\delta - t_\sigma) \\ \sqrt{3}(t_\delta - t_\sigma) & 3t_\sigma + t_\delta \end{pmatrix}$$

$$t_y = -\frac{1}{4} \begin{pmatrix} t_\sigma + 3t_\delta & \sqrt{3}(t_\sigma - t_\delta) \\ \sqrt{3}(t_\sigma - t_\delta) & 3t_\sigma + t_\delta \end{pmatrix}$$

$$t_z = -\begin{pmatrix} t_\sigma & 0 \\ 0 & t_\delta \end{pmatrix}$$

Note: t_σ includes predominantly the hopping via the intermediate oxygen while t_δ arises from the direct overlap and is small, which can be set 0 approximately.

- The next-nearest neighbor hopping matrices:

$$t_{xy} = \begin{pmatrix} -t'/2 & 0 \\ 0 & 3t'/2 \end{pmatrix}$$

$$t_{yz} = \begin{pmatrix} t' & \sqrt{3}t'/2 \\ \sqrt{3}t'/2 & 0 \end{pmatrix}$$

$$t_{zx} = \begin{pmatrix} t' & -\sqrt{3}t'/2 \\ -\sqrt{3}t'/2 & 0 \end{pmatrix}$$

- The tight-binding Hamiltonian on honeycomb lattice

$$\hat{H}(\vec{k}) = \begin{pmatrix} H_{AA}(\vec{k}) & H_{AB}(\vec{k}) \\ H_{BA}(\vec{k}) & H_{BB}(\vec{k}) \end{pmatrix}$$

with

$$H_{AA}(\vec{k}) = H_{BB}(\vec{k}) = 2[t_{xy}\cos(\vec{k} \cdot \vec{a}_1) + t_{zx}\cos(\vec{k} \cdot \vec{a}_2) + t_{yz}\cos(\vec{k} \cdot \vec{a}_3)]$$

$$H_{AB}(\vec{k}) = H_{BA}^\dagger(\vec{k}) = t_x e^{-i\vec{k} \cdot \vec{a}_2} + t_y e^{-i\vec{k} \cdot \vec{a}_3} + t_z$$

- By substituting the NN hopping matrix and NNN hopping matrix into the Hamiltonian, it can be written explicitly as:

$$\hat{H}(\vec{k}) = \begin{pmatrix} \tilde{\epsilon}_{aak} & \tilde{\epsilon}_{abk} & \epsilon_{aak} & \epsilon_{abk} \\ \tilde{\epsilon}_{abk} & \tilde{\epsilon}_{bbk} & \epsilon_{abk} & \epsilon_{bbk} \\ \epsilon_{aak}^* & \epsilon_{abk}^* & \tilde{\epsilon}_{aak} & \tilde{\epsilon}_{abk} \\ \epsilon_{abk}^* & \epsilon_{bbk}^* & \tilde{\epsilon}_{abk} & \tilde{\epsilon}_{bbk} \end{pmatrix}$$

with the matrix elements given by

$$\begin{aligned} \epsilon_{aak} &= -t_\sigma = \frac{1}{2} (t_\sigma + 3t_\delta) \cos(\sqrt{3}k_x/2) e^{-i3k_y/2} \\ \epsilon_{bbk} &= -t_\delta = \frac{1}{2} (t_\delta + 3t_\sigma) \cos(\sqrt{3}k_x/2) e^{-i3k_y/2} \\ \epsilon_{abk} &= -i \frac{\sqrt{3}}{2} (t_\sigma - t_\delta) \sin(\sqrt{3}k_x/2) e^{-i3k_y/2} \\ \tilde{\epsilon}_{aak} &= t' [4\cos(\sqrt{3}k_x/2)\cos(3k_y/2) - \cos(\sqrt{3}k_x)] \\ \tilde{\epsilon}_{bbk} &= 3t' \cos(\sqrt{3}k_x) \\ \tilde{\epsilon}_{abk} &= 2\sqrt{3}t' \sin(\sqrt{3}k_x/2)\sin(3k_y/2) \end{aligned}$$

where \mathbf{a}, \mathbf{b} are used to denote the two e_g orbitals with $|a\rangle = |d_{3x^2-y^2}\rangle$, $|b\rangle = |d_{x^2-y^2}\rangle$.

- By fitting the LDA band structure with tight-binding model parameters, previous studies[A.Rueegg, C.Mitra, et al_2012_PRB] show the dominant effect is from the nearest neighbor hopping $t_\sigma \approx 0.6\text{eV}$, the next biggest contribution is from next-nearest neighbor hopping $t' \approx 0.1t_\sigma$.

2.4 Periodic driven under a Laser field

1. Adding laser fields

- circularly polarized laser fields

$$\vec{A}(t) = A_0 = [\cos(\Omega t), -\sin(\Omega t)]$$

- linearly polarized laser fields

$$\vec{A}(t) = A_0 \cos(\Omega t) [\cos\theta, \sin\theta]$$

where A_0 and Ω are the amplitude and frequency of the laser, respectively.

2. Hamiltonian under laser field

- the canonical momentum of the electron is modified through the minimal substitution, $\vec{k} \rightarrow \vec{k} + \vec{A}(t)$, where $\vec{A}(t) = e\vec{A}(t)/\hbar$ with $\vec{A}(t)$ the in-plane laser vector potential, when the system is exposed to a normally incident laser field.
- Hamiltonian becomes time-dependent:

$$\hat{H}(\vec{k}, t) = \begin{pmatrix} H_{AA}(\vec{k}, t) & H_{AB}(\vec{k}, t) \\ H_{BA}(\vec{k}, t) & H_{BB}(\vec{k}, t) \end{pmatrix}$$

where we use the Coulomb gauge $\nabla\phi = 0$, and

$$H_{AB}(\vec{k}, t) = t_x e^{-i\vec{k}\cdot\vec{a}_2 - i\vec{A}\cdot\delta_z} + t_y e^{-i\vec{k}\cdot\vec{a}_3 - i\vec{A}\cdot\delta_y} + t_z e^{-i\vec{A}\cdot\delta_z}$$

3. Floquet theory

- Based on Floquet theory, the solution to the time-dependent Schrodinger equation can be expressed as:

$$|\psi(t)\rangle = e^{-i\epsilon_{k\alpha}t} |\phi_{k\alpha}(t)\rangle = e^{-i\epsilon_{k\alpha}t} \sum_m e^{im\Omega t} |\tilde{\phi}_{k\alpha}^m\rangle \quad m = 0, \pm 1, \pm 2, \dots$$

where we take a Fourier expansion, then,

$$\sum_m (H_{nm} + m\hbar\Omega\delta_{nm}) |\tilde{\phi}_{k\alpha}^m\rangle = \epsilon_{k\alpha} |\tilde{\phi}_{k\alpha}^m\rangle$$

with matrix elements of the Floquet Hamiltonian written as

$$H_{nm}(\vec{k}) = \frac{1}{T} \int_0^T dt e^{-i(n-m)\Omega t} H(\vec{k}, t)$$

$$= \begin{pmatrix} H_{nm}^{AA}(\vec{k}) & H_{nm}^{AB}(\vec{k}) \\ H_{nm}^{BA}(\vec{k}) & H_{nm}^{BB}(\vec{k}) \end{pmatrix}$$

- The rotating-wave approximation

In the **off-resonant** regime, a truncation of the Floquet components to be in $\mathbf{m}, \mathbf{n} = -2, -1, 0, 1, 2$ is a good approximation;

In the **on-resonant** regime, a truncation of the Floquet components \mathbf{m}, \mathbf{n} needs to be tested until convergence is achieved.

3 The quantitatively discription of energy bands with different parameters

1. Overview of the whole plan

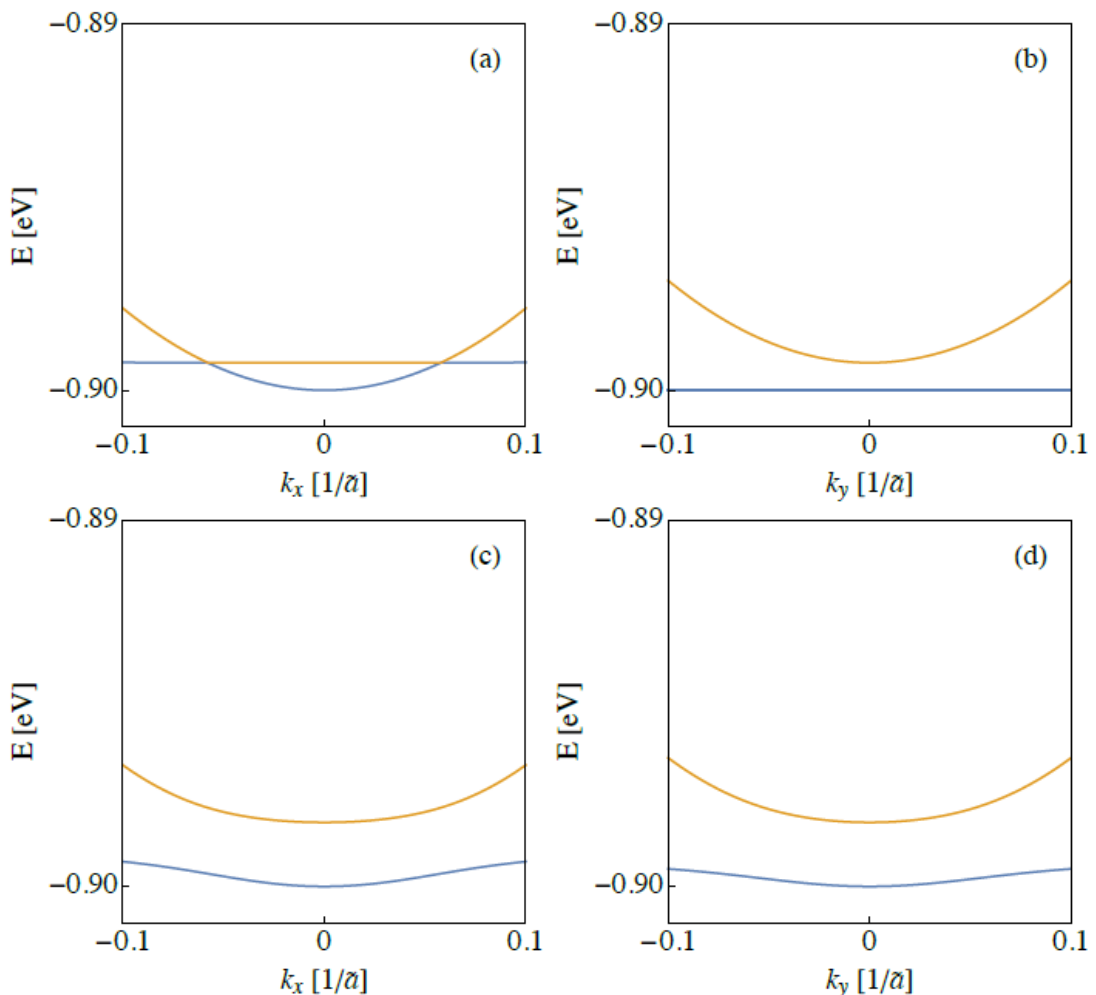
		Linearly φ	Circularly φ
$t_\sigma = 0.6\text{eV}$	Low-energy Resonant φ	1 φ	3 φ
	High-energy Off-resonant φ	2 φ	4 φ
$t_\sigma = 0.6\text{eV}$	Low-energy Resonant φ	5 φ	— φ
	High-energy Off-resonant φ	— φ	6 φ

2. $t_\sigma = 0.6\text{eV}, t' = 0.0\text{eV}$

- Linearly polarized light in a low-energy resonant regime:

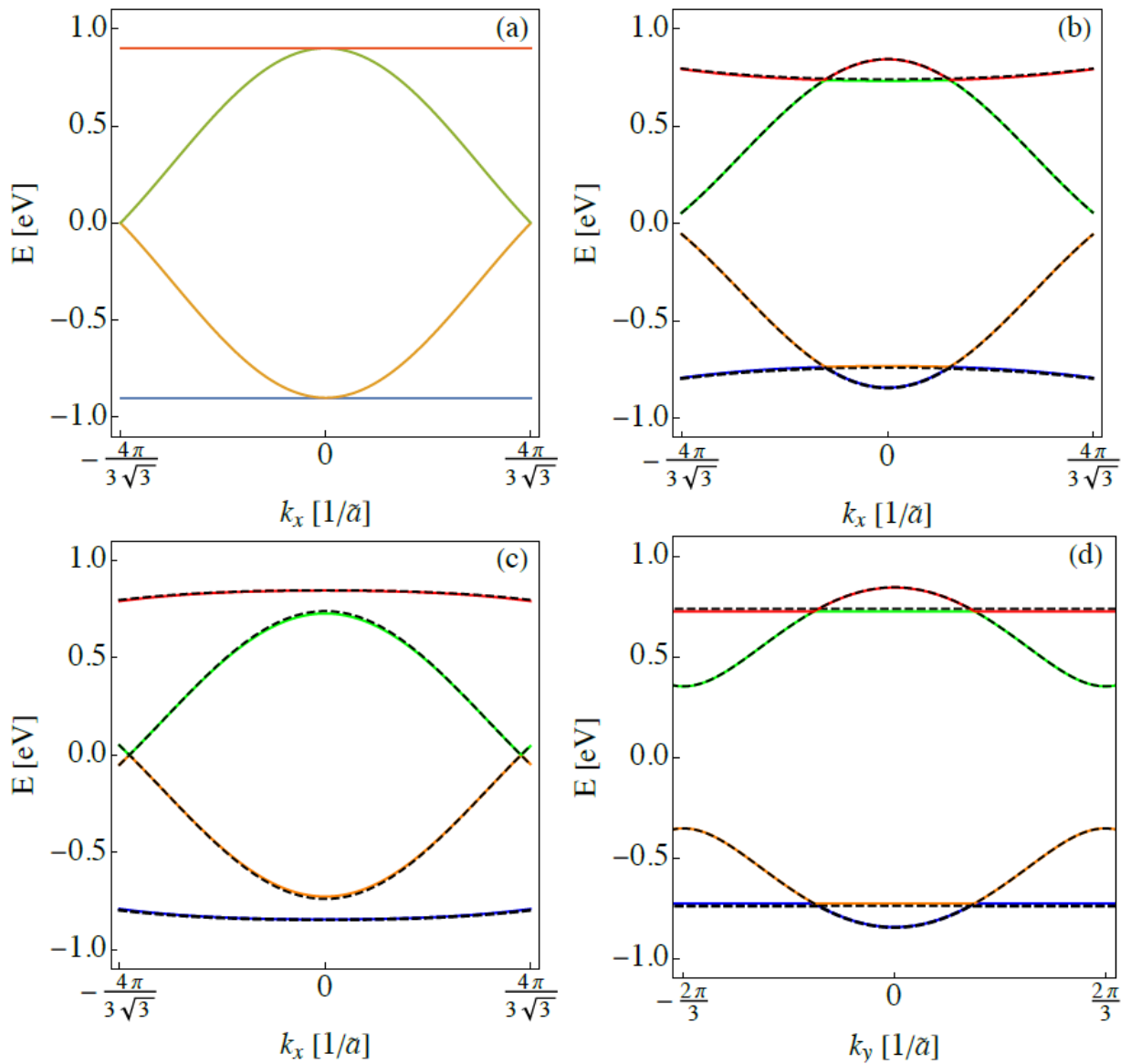
$$\tilde{A}_0 \tilde{a} = \sqrt{2}/10, \quad \hbar\Omega = 20.6783\text{meV} \quad (\nu = \Omega/2\pi = 5\text{THz}, I = 116.598\text{mW}/\mu\text{m}^2)$$

$$(a)\theta = 0; \quad (b)\theta = 0; \quad (c)\theta = \pi/2; \quad (d)\theta = \pi/2$$



- Linearly polarized light in a high-energy off-resonant regime:

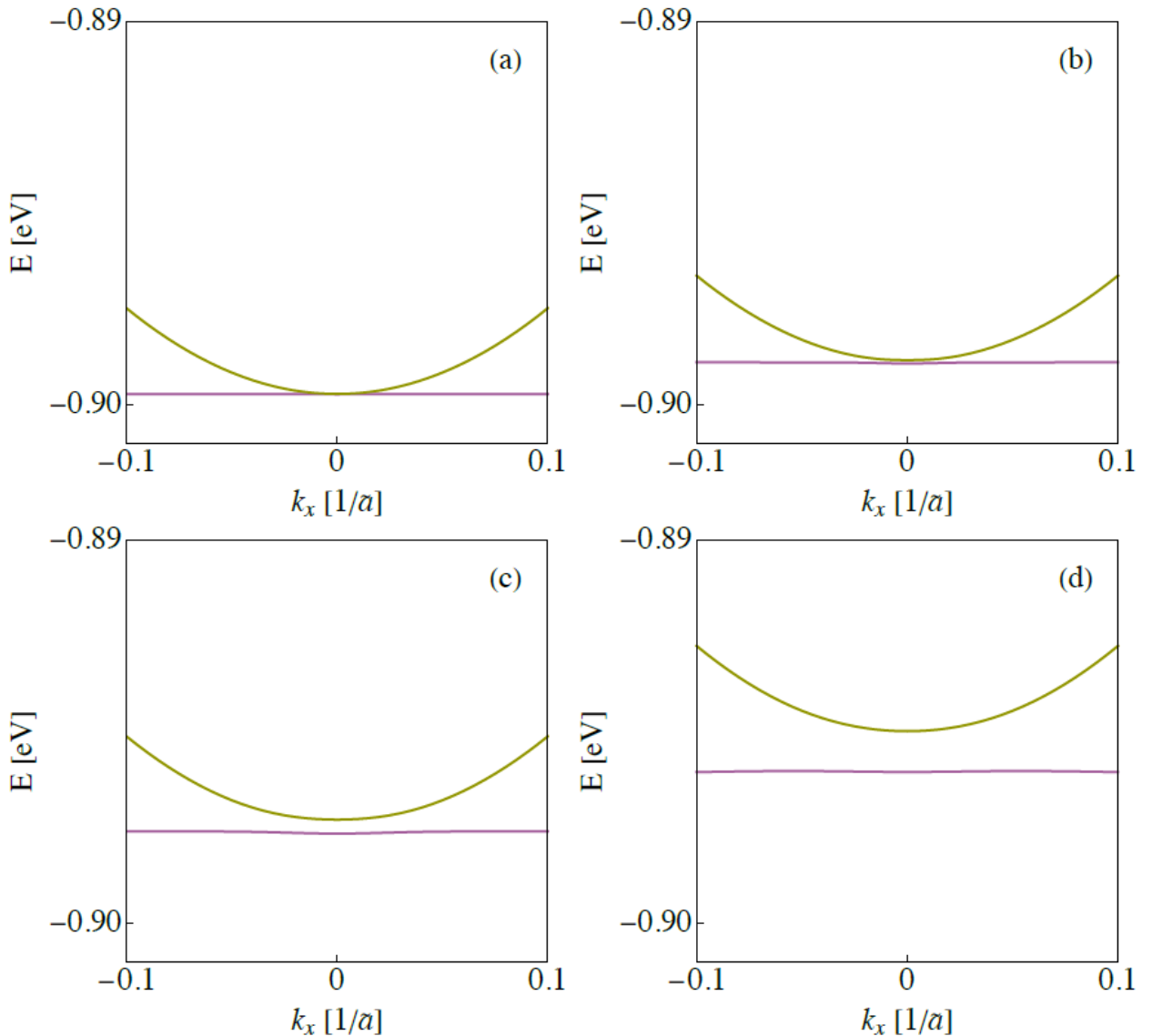
$$\tilde{A}_0 \tilde{a} = 1, \quad \hbar\Omega/t_\sigma = 10 \quad (\nu = \Omega/2\pi = 1.45079 \times 10^3 THz, I = 4.87887 \times 10^8 mW/\mu m^2)$$



- Circularly polarized light in a low-energy resonant regime:

$$\hbar\Omega = 20.6785 meV \quad (\nu = \Omega/2\pi = 5 THz)$$

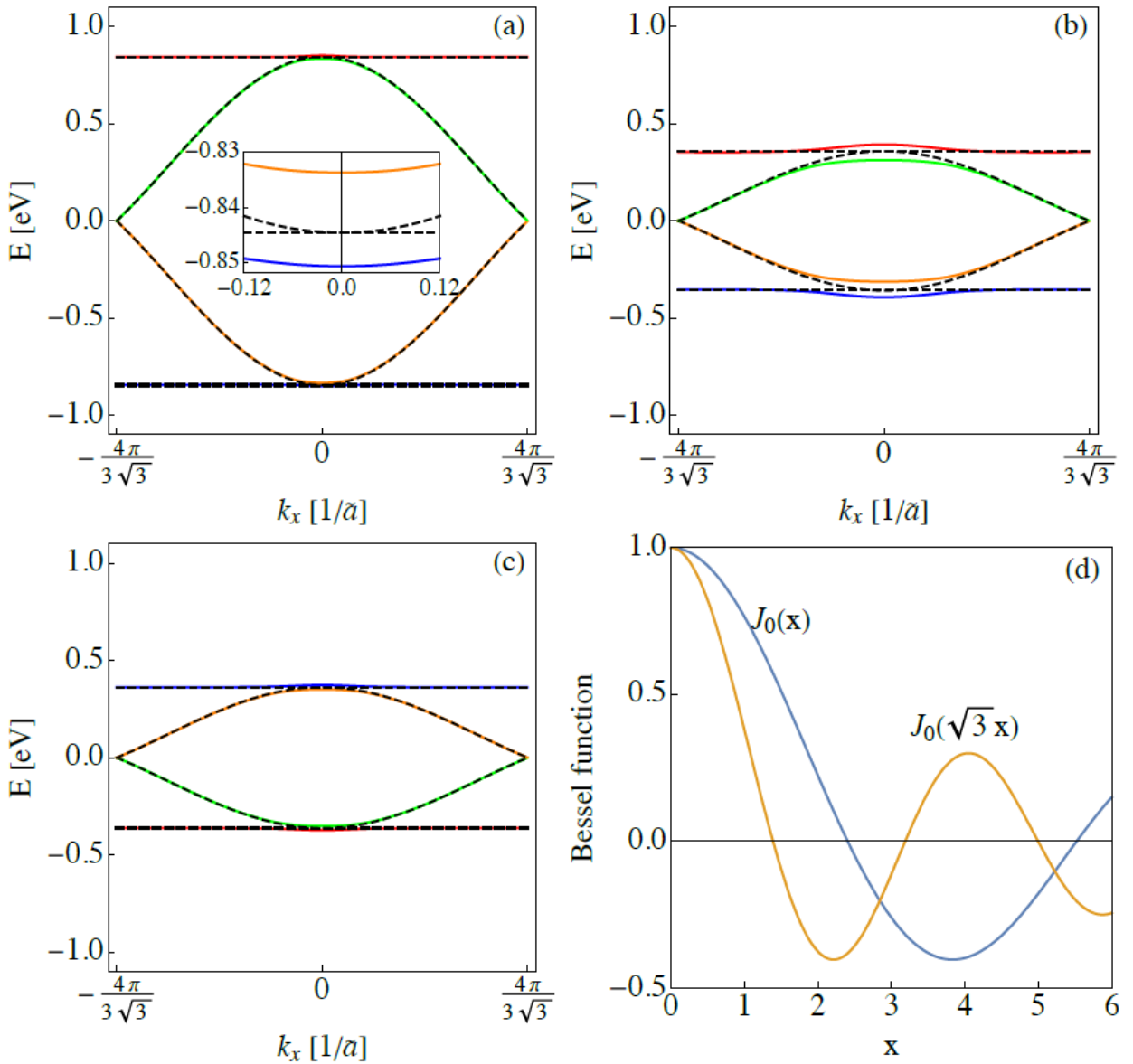
$$(a) \tilde{A}_0 \tilde{a} = 0.05 \quad (I = 14.57457 mW/\mu m^2) \quad (b) \tilde{A}_0 \tilde{a} = 0.10 \quad (I = 58.299 mW/\mu m^2) \\ (c) \tilde{A}_0 \tilde{a} = 0.15 \quad (I = 131.17275 mW/\mu m^2) \quad (d) \tilde{A}_0 \tilde{a} = 0.20 \quad (I = 233.196 mW/\mu m^2)$$



- Circularly polarized light in a high-energy off-resonant regime:

$$\hbar\Omega/t_\sigma = 10 \quad (\nu = \Omega/2\pi = 1.45079 \times 10^3 \text{ THz})$$

- (a) $\tilde{A}_0 \tilde{a} = 0.5$ ($I = 1.21972 \times 10^8 \text{ mW}/\mu\text{m}^2$), the inset shows a zoomed view around the quadratic band touching at 1/4 filling
- (b) $\tilde{A}_0 \tilde{a} = 0.10$ ($I = 58.299 \text{ mW}/\mu\text{m}^2$)
- (c) $\tilde{A}_0 \tilde{a} = 0.15$ ($I = 131.17275 \text{ mW}/\mu\text{m}^2$)
- (d) The zero – th order Bessel function of the first kind

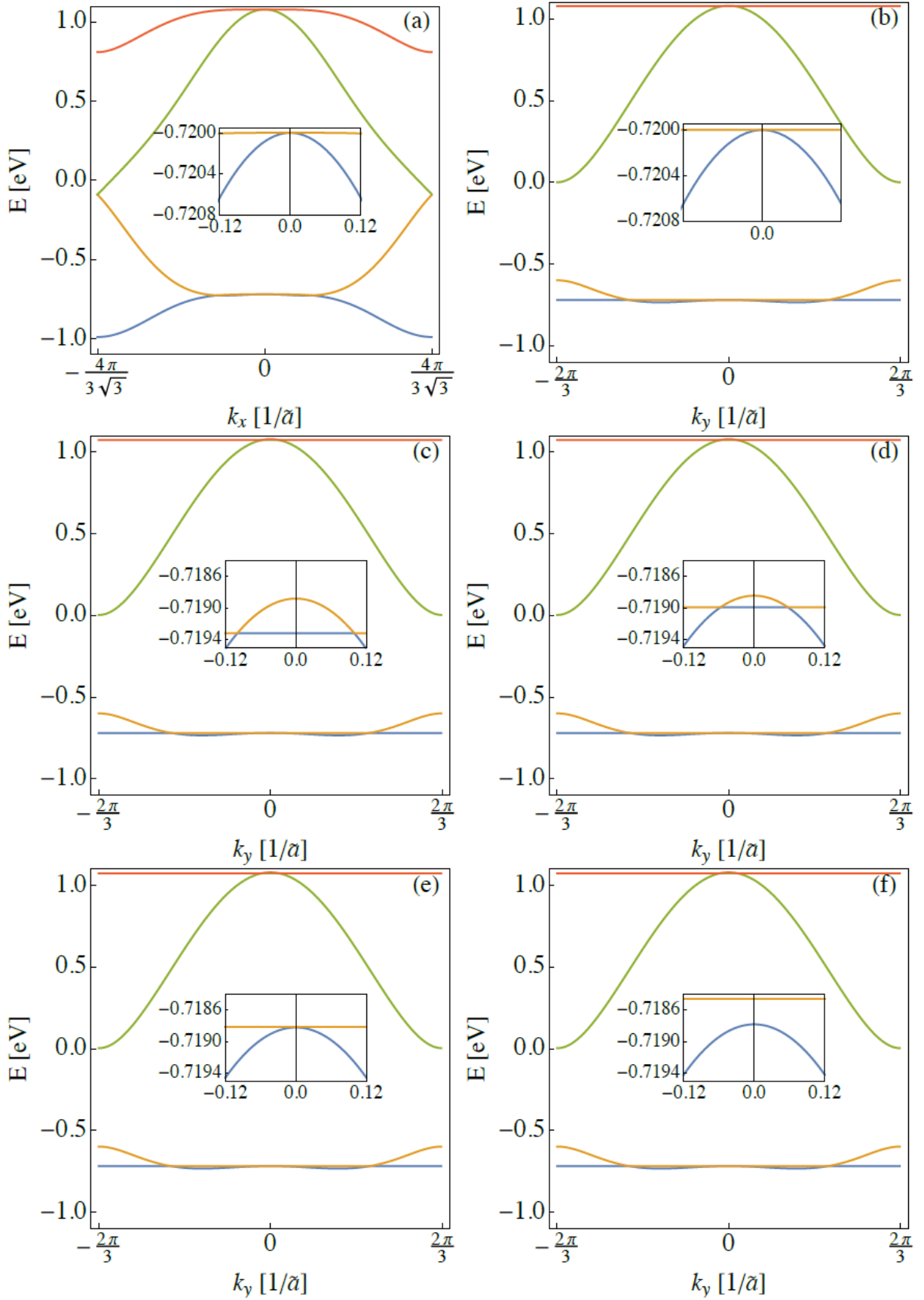


$$3. t_\sigma = 0.6 \text{ eV}, t' = 0.1 t_\sigma$$

- Linearly polarized light in a low-energy resonant regime:

$$\tilde{A}_0 \tilde{a} = \sqrt{2}/10, \quad \theta = 0$$

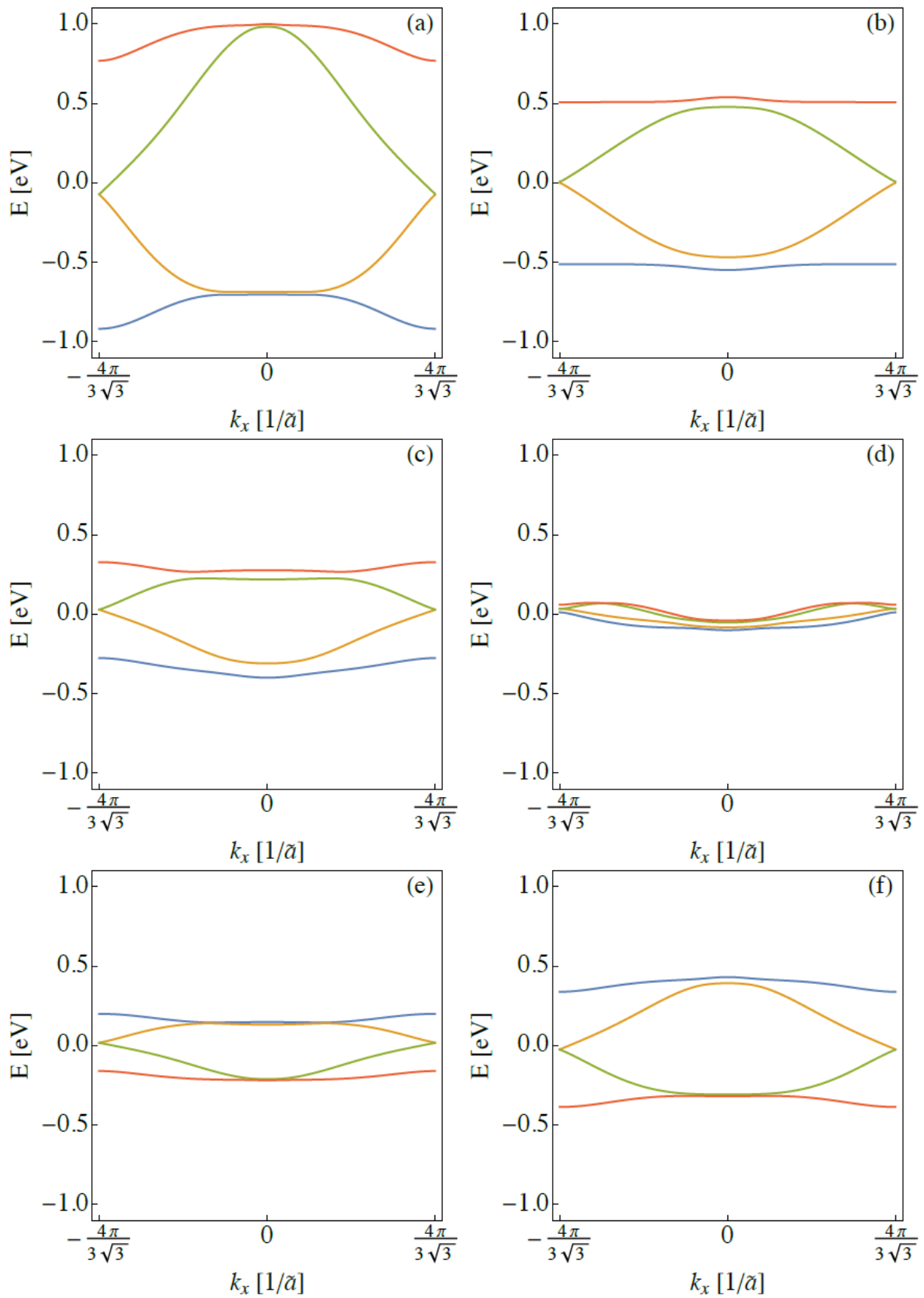
- (a) bands along k_x , abense of laser
- (b) bands along k_y , absense of laser
- (c) $\hbar\Omega/t_\sigma = 100$, $\nu = 14.5079 \times 10^3 \text{ THz}$, $I = 9.75774 \times 10^8 \text{ mW}/\mu\text{m}^2$
- (d) $\hbar\Omega/t_\sigma = 10.0$, $\nu = 1.45079 \times 10^3 \text{ THz}$, $I = 9.75774 \times 10^6 \text{ mW}/\mu\text{m}^2$
- (e) $\hbar\Omega/t_\sigma = 8.33$, $\nu = 1.20899 \times 10^3 \text{ THz}$, $I = 6.77621 \times 10^6 \text{ mW}/\mu\text{m}^2$
- (f) $\hbar\Omega/t_\sigma = 6.77$, $\nu = 0.96719 \times 10^3 \text{ THz}$, $I = 4.33677 \times 10^6 \text{ mW}/\mu\text{m}^2$



- Circularly polarized light in a high-energy off-resonant regime:

$$\hbar\Omega/t_\sigma = 10 \quad (\nu = \Omega/2\pi = 1.45079 \times 10^3 \text{ THz})$$

- (a) $\tilde{A}_0 \tilde{a} = 0.50, \quad I = 1.21972 \times 10^8 \text{ mW}/\mu\text{m}^2$
- (b) $\tilde{A}_0 \tilde{a} = 1.39, \quad I = 9.42646 \times 10^8 \text{ mW}/\mu\text{m}^2$
- (c) $\tilde{A}_0 \tilde{a} = 1.80, \quad I = 1.58075 \times 10^9 \text{ mW}/\mu\text{m}^2$
- (d) $\tilde{A}_0 \tilde{a} = 2.40, \quad I = 2.81023 \times 10^9 \text{ mW}/\mu\text{m}^2$
- (e) $\tilde{A}_0 \tilde{a} = 2.83, \quad I = 3.90744 \times 10^9 \text{ mW}/\mu\text{m}^2$
- (e) $\tilde{A}_0 \tilde{a} = 3.80, \quad I = 7.04509 \times 10^9 \text{ mW}/\mu\text{m}^2$



4. The solid lines for Nickel-Nickel tight-binding and the dashed lines for Nickel-Oxygen tight-binding model

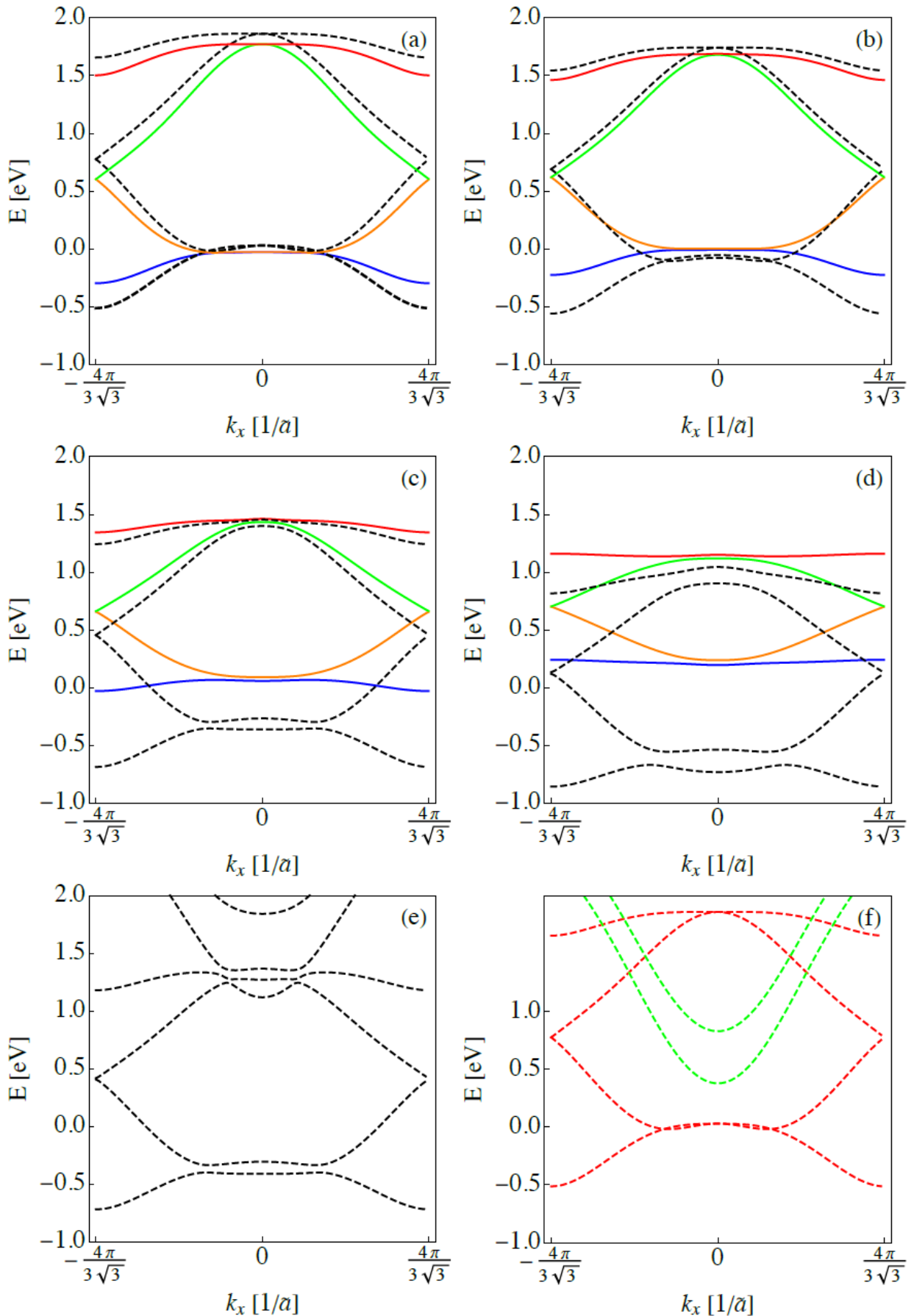
$$\vec{A}(t) = A_0(\cos\Omega t, -\sin\Omega t), \quad t_\sigma = 0.6eV, \quad t' = 0.1t_\sigma$$

(a) Equilibrium

$$(b) \tilde{A}_0 \tilde{a} = 0.50, \quad \hbar\Omega = 12eV$$

$$(c) \tilde{A}_0 \tilde{a} = 1.00, \quad \hbar\Omega = 12eV \quad (d) \tilde{A}_0 \tilde{a} = 1.50, \quad \hbar\Omega = 12eV$$

$$(e) \tilde{A}_0 \tilde{a} = 1.00, \quad \hbar\Omega = 10.5eV \quad (f) \tilde{A}_0 \tilde{a} = 0.00, \quad \hbar\Omega = 10.5eV$$



4 Semiconductor quantum well structure

4.1 Basic features of HgCdTe quantum well

4.2 model and method

4.3 Experimental realization

1. Magnetic field
2. Stress modulation
3. Electric field

5 Preliminary Knowledge

5.1 The inverted energy level in HgTe

5.2 Slater-Koster method

[J. C. Slater, G. F. Koster_1957_*Simplified LCAO Method for the Periodic Potential Problem*]

1. The LACO Method for Solids
2. Simplification of the LACO Method
3. The Two-Center Approximation
4. The Simple Cubic structure
5. The Face-centered cubic structure
6. The Body-centered cubic structure
7. The Diamond structure

5.3 The rotating-wave approximation